Reactive scattering of H2 on Cu(111) at 925 K: effective Hartree potential vs sudden approximation

Smits, B.; Sah Mantu, K.; Naskar, K.; Adhikari, S.; Meyer, J.; Somers, M.F.

RESEARCH ARTICLE | OCTOBER 15 2024

Reactive scattering of H_2 on Cu(111) at 925 K: Effective Hartree potential vs sudden approximation

Bauke Smits ; Mantu Kumar Sah ; Koushik Naskar ; Satrajit Adhikari ; Jörg Meyer ; Mark F. Somers

J. Chem. Phys. 161, 154702 (2024)
https://doi.org/10.1063/5.0231559

The Journal of Chemical Physics ARTICLE pubs.aip.org/aip/jcp

Reactive scattering of H_2 on Cu(111) at 925 K: Effective Hartree potential vs sudden approximation

Cite as: J. Chem. Phys. 161, 154702 (2024); doi: 10.1063/5.0231559
Submitted: 31 July 2024 • Accepted: 29 September 2024 •
Published Online: 15 October 2024

Bauke Smits,[1,a] Mantu Kumar Sah,[2] Koushik Naskar,[2] Satrajit Adhikari,[2] Jörg Meyer,[1,b] and Mark F. Somers[1,c]

AFFILIATIONS

[1] Leiden Institute of Chemistry, Gorlaeus Building, Leiden University, P.O. Box 9502, 2300 RA Leiden, The Netherlands
[2] School of Chemical Sciences, Indian Association for the Cultivation of Science, Jadavpur, Kolkata 700032, India

[a] Electronic mail: b.smits@lic.leidenuniv.nl
[b] Electronic mail: j.meyer@chem.leidenuniv.nl
[c] Author to whom correspondence should be addressed: m.somers@chem.leidenuniv.nl

ABSTRACT

We present new quantum dynamical results for the reactive scattering of hydrogen molecules from a Cu(111) surface at a surface temperature of 925 K. Reaction, scattering, and diffraction probabilities are compared for results obtained using both an effective Hartree potential (EfHP) and a sudden approximation approach, implemented through the static corrugation model (SCM), to include surface temperature effects. Toward this goal, we show how the SRP48 DFT-functional and an embedded atom potential perform when used to calculate copper lattice constants and thermal expansion coefficients based on lattice dynamics calculations within the quasi-harmonic approximation. The so-calculated phonons are then used in the EfHP approach to replace the normal modes of a fictitious copper cluster used in earlier work. We find that both the EfHP and SCM approaches correctly predict the reaction probability curve broadening effect when the surface temperature is increased. Similarly, results for rovibrationally elastic scattering appear to be improved, predominantly for the SCM model. The behavior of the EfHP results appears to remain much closer to that of a Born–Oppenheimer static surface approach, which excludes any surface temperature effects. Finally, for the diffraction, we show very clear attenuation effects for the SCM approach, significantly decreasing specular diffraction probabilities at 925 K surface temperature. These results demonstrate that state-of-the-art theoretical models are able to reproduce strictly quantum mechanical scattering effects with a sudden approximation model and open up interesting opportunities for further comparisons to experimental diffraction results.

I. INTRODUCTION

The dissociation of small molecules on metal surfaces is one of the most important topics in the field of surface science, due to its prevalence as the rate-limiting step in industrial processes such as the Haber–Bosch process[1] (N_2 on Fe) or methane steam reforming[2] (CH_4 on Ni). To ensure a large amount of available data when designing and developing new (theoretical) models to describe these reactions, a focus has been put on several characteristic model systems. One of these model systems is the reactive scattering of H_2 from a Cu(111) surface, which has a wide array of available experimental[3–11] and theoretical[12–32] data, making it an ideal model for further study.

When modeling the dynamics of these kinds of reactions at the atomic scale, theoretical work often ignores the effect of surface temperature, as it requires accounting for the motion of the surface atoms.[33–35] Nevertheless, several approaches have been suggested to include these surface temperature effects, such as seven-dimensional models by Jackson and co-workers for the dissociation of CH_4 (in reduced dimensions), where a single degree-of-freedom (DoF) was used to describe surface motion.[36,37] This approach was similarly applied as a sudden approximation model with statically

distorted surfaces. Jackson has also developed a reduced density matrix (RDM)[38] approach, modeling the surface as a phonon bath, which was used to investigate the effects of surface temperature on methane trapping on a metal surface.[39,40] Furthermore, Busnengo and co-workers also made use of what is referred to as a static distorted surface (SDS) model, another sudden approximation approach, as well as moving surface dynamics for the dissociation of CH_4 at elevated surface temperatures, all performed at a classical level using a reactive force-field based approach.[41–43] Kroes *et al.* introduced a static disorder parameter, which shifts the reaction probability curves with a single factor based on surface temperature.[44] Meyer and Reuter introduced a QM/Me embedding approach, disentangling the substrate–substrate and substrate–adsorbate interactions to describe energy dissipation to the surface.[45] As a more general approach, high-dimensional neural network potentials (HD-NNPs)[22,46–50] and ring polymer molecular dynamics[51,52] have seen a huge rise in the field recently, being applied to a variety of atom–surface combinations while being capable of including surface motion to some effect. Finally, the static corrugation model (SCM), originally proposed by Wijzenbroek and Somers,[15] introduced a simple coupling potential to describe the effect of a static, but thermally distorted, surface slab on the H_2/Cu(111) reaction for classical dynamics. This sudden approximation approach was later expanded by Smits *et al.*[28] to also be implemented in time-dependent wave packet (TDWP) calculations. This was the first model, to our knowledge, to have been shown to accurately reproduce experimental results using fully 6D quantum dynamics simulations,[29,31] although reduced dimensionality studies have been performed in the past with limited accuracy.[53] Another method using the same TDWP code and same SCM coupling potential was introduced by Adhikari and co-workers in the form of the effective Hartree potential approach (EfHP). Here, the effect of the surface motion is described using a coupling to a bath of Cu-cluster normal modes, using an effective Hartree potential.[27,30,32]

Previous studies with this EfHP approach always relied on describing the displacements of the Cu surface using the normal modes of a small 31 atom copper cluster.[27,30] These studies, however, still found significant differences between dissociation probabilities obtained using the EfHP experiment and some of the other approaches discussed. As the frequency distributions of the atom displacements in these clusters vary significantly from those one would expect for a fully infinite surface, we believe further improvements could be made by instead obtaining these vibrational modes from calculations taking into account the infinite nature of the surface. In addition, as the EfHP is based on a phonon or normal mode description of the surface bath, the model has the inherent property that it cannot describe thermal lattice expansion by itself. Furthermore, recent work on the EfHP has found several improvements to its implementation that could improve its accuracy. Thus, this is an ideal time to revisit and further improve upon the EfHP approach by replacing the cluster-obtained normal modes with a more accurate description of the Cu(111) surface and by investigating the role of thermal expansion of the solid.

In this study, we will investigate the reactive scattering of H_2 from a (thermally excited) Cu(111) surface at a quantum dynamical level using the EfHP approach by combining it with a phonon approximation to describe the surface. Although the phonon calculations themselves can be performed quite straightforwardly, some attention will have to be paid to the lattice constant of the surface we will be interested in using, as well as how this aligns with the lattice constant used for the ideal Born–Oppenheimer static surface (BOSS) PES, which is modified by the EfHP approach. In addition, we will pay some attention to which BOSS PES to use precisely and how in order to properly account for the thermal lattice expansion effects on the H_2 to dissociation barrier. Having decided upon several surface descriptions, we will compare the phonon frequencies we obtain to those of the normal modes used in the previous studies. Finally, we will look at several dynamics results in the form of reaction, scattering, and diffraction probabilities, comparing the EfHP results to those obtained from the ideal lattice BOSS approach, as well as a sudden approximation approach from the SCM, and finally, some experimental results where available. The SCM was chosen in particular due to our experience with the model as well as its great agreement with the available experimental results, even at a quantum dynamical level.[28,29,31] Furthermore, previous work has shown that electron–hole pair excitations play a minimal role in the H_2/Cu(111) system, so they will be neglected in this study.[20]

II. METHODS

A. Quantum dynamics

We performed 6D QD simulations using the time-dependent wave packet (TDWP) approach to solve the corresponding Schrödinger equation. The full Hamiltonian of the system can be written as

$$\hat{H}(\vec{Q}) = -\frac{\hbar^2}{2M}\nabla^2_{\vec{R}} - \frac{\hbar^2}{2\mu r^2}\frac{\partial^2}{\partial r^2} + \frac{1}{2\mu r^2}\hat{J}^2(\theta,\phi) + V_0(\vec{q_0},\vec{r},\vec{R}) + V_{Temp}(\vec{Q}). \quad (1)$$

Here, M and μ describe the mass and reduced mass of the hydrogen molecule, respectively. ∇ and $\hat{J}$ describe the linear and angular momentum operators, respectively; and V_0 represents the ideal 6D PES of our surface. $\vec{r}(r,\theta,\phi)$ describes the bond distance and angular orientation of the H_2 molecule, and $\vec{R}(X,Y,Z)$ the coordinates of its center of mass. $\vec{Q} = (\vec{q},\vec{r},\vec{R})$ with $\vec{q}$ being the collective Cu surface atom degrees of freedom. V_0 is thus the BOSS ideal surface potential ($\vec{q_0}$ being the prefect lattice Cu positions at 0 K). The additional V_{Temp} is included to introduce surface temperature effects to the calculations using two different models (and, thus, implicitly depends on the choice made for V_0 and $\vec{q_0}$).

The first model is the SCM, a sudden approximation approach designed to include the relevant surface temperature effects in a computationally efficient manner.[15,21,28] Within this model, the change in potential due to the surface atoms being thermally distorted is included as a separate coupling potential,

$$V_{Temp} = V_{coup}(\vec{q_0} \to \vec{q},\vec{r},\vec{R}) + V_{strain}(\vec{q_0} \to \vec{q}). \quad (2)$$

V_{coup} is thus the change in energy in the H_2–Cu interaction potential, and V_{strain} is the change in Cu–Cu interaction potential due to the thermal surface displacement from $\vec{q_0} \to \vec{q}$. However, as we use a sudden approximation approach, the V_{strain} can be neglected

in the dynamics of H_2. For this work, we describe V_{coup} using an effective three-body potential, as was first introduced by Spiering *et al.*,[21] and which was shown to accurately reproduce experimental results for this system[24,28,29,31] when combined with surface configurations obtained from an accurate surface potential, even at a quantum dynamical level.

Results from the SCM model are compared to those obtained using the EfHP approach introduced by Adhikari and coworkers.[27,30,32] For the latter, the potential is expanded as

$$V_{Temp} = V_{eff}^{vib}(\vec{r}, \vec{R}, t, T_s), \tag{3}$$

introducing both a time and a temperature dependence to the calculations. To include the effects of surface temperature, or more specifically, surface atom vibrations, into the model, the full system is now described as a Hartree product type of wavefunction,

$$\Psi(\vec{r}, \vec{R}, t) \cdot \Phi_{vib}(\{Q_k\}, t) \tag{4}$$

with the surface described by a bath of surface vibrations (Φ), depending on the surface normal modes ($\{Q_k\}$). The potential of the surface vibrations is described using

$$V_{eff}^{vib}(\vec{r}, \vec{R}, t, T_s) = \sum_{\{n_0\}} p_{\{n_0\}} \langle V \rangle_{\{n_0\}}^{vib}, \tag{5}$$

with p being the probability distribution of the vibrational state population, either in a Bose–Einstein or Maxwell–Boltzmann distribution, and $\{n_0\}$ being the collection of vibrational configurations. The Hartree potential for each of these configurations can be described by

$$\langle V \rangle_{\{n_0\}}^{vib} = \left\langle \Phi_{vib} | V_I^{vib} | \Phi_{vib} \right\rangle, \tag{6}$$

with V_I^{vib} being the interaction potential between the molecular and surface DoFs. In this work, the effective three-body SCM potential (V_{coup}) by Spiering, Wijzenbroek, and Somers[21] is employed. A more thorough description of the EfHP model can be found in Refs. 27, 30, and 32.

For all of the quantum-dynamical calculations with both models, the initial wave function $\Psi(\vec{r}, \vec{R}, t = 0)$ is represented as the product of a rovibrational wave function $[\psi_{v,j,m_j}(r, \theta, \phi)]$ of the H_2, a two-dimensional plane wave function $[\phi(k_0^X, k_0^Y)]$ along X and Y, and a Gaussian wave packet $[u(Z; Z_0, k_0^Z)]$ centered around a point far away from the surface,

$$\Psi(\vec{r}, \vec{R}, t = 0) = \psi_{v,j,m_j}(r, \theta, \phi)\phi(k_0^X, k_0^Y)u(Z; Z_0, k_0^Z). \tag{7}$$

The wave-packets are propagated using the split-operator (SPO) method,[54] while optical potentials of a quadratic form are added to both the scattering and reactive channel regions,[55] absorbing the wave-packet after analysis. The scattered fraction is analyzed using the scattering matrix formalism at a point at large Z,[56] which yields the scattering probabilities for each rovibrational state and diffraction channel separately. The sticking probability is subsequently calculated by subtracting the sum of all these scattering probabilities from the total possible probability of unity. At the same time, a flux analysis in r, directly measuring the flux through a plane for a specific large value of r, is performed, which also yields dissociation probabilities but provides no information on the scattered states. For a more in-depth discussion of the basis of these quantum mechanical methods, we direct the reader to Refs. 57 and 58.

B. Phonons and quasi-harmonic approximation

The total internal energy of a perfect surface (without defects) can be expanded in displacement coordinates $\vec{u} = \vec{q} - \vec{q}_0$ around the equilibrium positions of the Cu atoms. Terminating this expansion after the second order is called the harmonic approximation,

$$V^{\text{harm}}(\vec{u}) = V^{\text{eq}} + \frac{1}{2}\sum_{n,i,\alpha}\sum_{n',i',\alpha'} \Phi_{n,i,\alpha}^{n',i',\alpha'}\, u_{n,i,\alpha}\, u_{n',i',\alpha'}. \tag{8}$$

Here, the summations extend over the infinitely many unit cells describing the surface (n'), the N_{cell} atoms within a surface unit cell ($i' = 1, \ldots, N_{\text{cell}}$), and their Cartesian coordinates ($\alpha' = 1, 2, 3$). $u_{n,i,\alpha}$ denotes the displacement along the Cartesian direction α of atom i in a replica n. In the following, $V^{\text{eq}} = V(\vec{u} = \vec{0})$ is chosen as energy zero such that it does not need to be explicitly denoted. This only leaves the second order (or so-called harmonic) term, which is fully defined by the force constants $\Phi_{n,i,\alpha}^{n',i',\alpha'}$. The forces in the harmonic approximation are given by

$$F_{n,i,\alpha}^{\text{harm}} = -\frac{\partial E^{\text{harm}}}{\partial u_{n,i,\alpha}} = -\sum_{n',i',\alpha'} \Phi_{n,i,\alpha}^{n',i',\alpha'} u_{n',i',\alpha'}, \tag{9}$$

resulting in the following Newtonian equations of motion:

$$-\sum_{n',i',\alpha'} \Phi_{n,i,\alpha}^{n',i',\alpha'} u_{n',i',\alpha'} = M_i \frac{\partial^2 u_{n,i,\alpha}}{\partial t^2} \tag{10}$$

for each atom in the Cu(111) surface with mass $M_i = M_{\text{Cu}} = 63.546$ u. In principle, the force constant matrix $\Phi_{n,i,\alpha}^{n',i',\alpha'}$ couples the motion of all atoms in the crystal, with the strength of the couplings typically decreasing with increasing distance from a reference atom. Equation (10) can be solved by the following plane wave-like ansatz for the displacement patterns:

$$u_{n,i,\alpha}(\vec{k}, t) = \frac{A}{\sqrt{M_i}}\, \tilde{u}_{i,\alpha}(\vec{k})\, \exp\left(i(\vec{k} \cdot \vec{q}_{0\,n,i} - \omega(\vec{k})t)\right), \tag{11}$$

where $\vec{q}_{0\,n,i}$ is the ideal lattice position of atom i in (replica) cell n. The wave vector $\vec{k}$ characterizes the periodicity of such a displacement pattern with (angular) frequency $\omega(\vec{k})$. All possible displacement patterns can be described by wave vectors that are contained in the (first) Brillouin zone of the crystal (Wigner–Seitz cell of the reciprocal lattice). The unit vector $\tilde{u}_{i,\alpha}(\vec{k})$ describes the displacements of each atom in a unit cell, and A is the amplitude of the resulting displacement pattern. Substitution of this ansatz into Eq. (10),

$$\omega^2 \tilde{u}_{i,\alpha}(\vec{k}) = \sum_{i',\alpha'} \sum_{n} \frac{1}{\sqrt{M_i M_{i'}}} \Phi^{n',i',\alpha'}_{n,i,\alpha} \tilde{u}_{i,\alpha}(\vec{k}) \exp(i\vec{k} \cdot \vec{q}_{0n,i}), \quad (12)$$

then allows to determine the frequencies $\omega(\vec{k})$ and directions of atomic displacements $\tilde{u}_{i,\alpha}(\vec{k})$ that are described by Eq. (11). Introducing the so-called dynamical matrix,

$$D^{i',\alpha'}_{i,\alpha}(\vec{k}) = \sum_{n} \frac{1}{\sqrt{M_i M_{i'}}} \Phi^{n',i',\alpha'}_{n,i,\alpha} \exp(i\vec{k} \cdot \vec{q}_{0n,i}). \quad (13)$$

Equation (12) constitutes an eigenvalue problem for this $3N_{\text{cell}} \times 3N_{\text{cell}}$ dimensional matrix,

$$\omega^2 \tilde{u}_{i,\alpha}(\vec{k}) = \sum_{i',\alpha'} D^{i',\alpha'}_{i,\alpha}(\vec{k}) \tilde{u}_{i,\alpha}(\vec{k}). \quad (14)$$

Since $D(\vec{k})$ is Hermitian it can be diagonalized and the $3N_{\text{cell}}$ different eigenvectors and concomitant eigenvalues provide solutions for the displacements $\vec{u}_j(\vec{k})$ and their concomitant frequencies $\omega_b(\vec{k})$, respectively, where $j = 1, \ldots, 3N_{\text{cell}}$. Each solution it describes is a particular phonon state. At each $\vec{k}$-point, these states are enumerated by the band index j, and the total amount of bands is determined by the amount of atoms in the primitive unit cell. In practice, solutions for a discrete set of $\vec{k}$-points sampling the Brillouin zone are being calculated.

Since the expectation value for the position of each phonon oscillator is zero, thermal expansion cannot be described by the harmonic approximation. The so-called quasi-harmonic approximation is a simple and computationally convenient extension of the harmonic approximation, which is able to describe thermal expansion. Substituting the equilibrium by general vectors lattice $(\{\vec{a}_0, \vec{b}_0, \vec{c}_0\} \rightarrow \{\vec{a}, \vec{b}, \vec{c}\})$ in Eq. (8) leads to lattice-vector-dependent or equivalently unit-cell-volume-dependent $(\Omega = \vec{a} \cdot (\vec{b} \times \vec{c}))$ force constants $\Phi^{n',i',\alpha'}_{n,i,\alpha}(\Omega)$. Consequently, also the solutions of the lattice dynamical equations [see Eq. (14)] change as a function of Ω, resulting in a phonon contribution to the Helmholtz free energy,

$$F^{\text{qh}}(T;\Omega) = \frac{1}{2} \sum_{\vec{k},j} \hbar\omega_j(\vec{k};\Omega) + k_B T \sum_{\vec{k},j} \ln\left[1 - \exp\left(\frac{-\hbar\omega_j(\vec{k};\Omega)}{k_B T}\right)\right] \quad (15)$$

that depends on both temperature T and Ω. Minimizing F^{qh} with respect to Ω for a given temperature results in $\Omega^{\text{qh}}(T)$. For a given potential that describes surface vibrations, the quasi-harmonic approximation thus allows us to describe the thermal expansion and inherently captures the influence of the expansion on the phonons of the surface.

C. Computational details

In this work, we will be comparing results obtained using several interaction potentials. The first is the BOSS approach, which has been a staple in the field of theoretical surface science for many years.[34,35] This is used as a baseline to compare where the surface atoms are frozen in their ideal lattice positions with their interaction with the H_2 molecule described using a PES. We will look at two different BOSS-obtained results; the first was fitted by Mondal *et al.* using the CRP approach,[59] with the single-point energies obtained using DFT with the semi-empirical SRP48 exchange–correlation functional.[18] Here, the lattice constant was taken from energy minimization using the SRP48 functional. This is thus a perfect lattice 0 K BOSS PES. The other was also fitted using the CRP, and DFT results were obtained using the SRP48 functional; however, here the lattice constant was expanded to better describe a 925 K Cu-lattice.[60] Thus, although surface temperature lattice distortions are not included, the thermal expansion is to some extent. It is thus a 925 K perfect lattice BOSS CRP PES.

The first of the interaction potentials that includes the relevant surface temperature effects is the SCM, a sudden approximation approach designed by Wijzenbroek and Somers.[15] In particular, we will compare the results by Smits *et al.*, who used an accurate embedded atom method (EAM) potential to describe the thermal surface distortions and were able to reproduce experimental results very well.[31] In that work, the 0 K perfect lattice BOSS CRP PES was used, and the thermal lattice expansion is included via the SCM approach: the H_2 X and Y center of mass coordinates are rescaled accordingly.[15]

We compare the EfHP approach by Adhikari *et al.*[27,30] Here, the system is coupled to a bath of surface modes, with the interaction described using the same SCM coupling potential used for the SCM. It is straightforward to employ the formalism and implementation described before[27,30] with the phonons calculated here: Frequencies and eigenvectors from these calculations using periodic boundary conditions [see Eq. (14)] can be directly substituted for the normal mode frequencies and displacements resulting from the previous cluster calculations. In practice, the discretization of the phonon spectrum is determined by the amount of phonons that are commensurate with the supercell (81 for bulk phonon calculations and 27 for the surface slab phonon calculations). We used the 0 K perfect lattice BOSS CRP PES when using the EAM based phonons and again rescaled the H_2 center of mass X and Y coordinates to account for lattice expansion, just like is done in SCM.[15] However, we use the 925 K perfect lattice BOSS CRP PES[60] without any rescaling of any H_2 coordinates when using the 925 K SRP48 phonons in the EfHP. This is to ensure a consistent quasi-harmonic picture of the system in which the thermal lattice expansion effects on the H_2 dissociation barrier are also included. When it comes to the dynamics of the surface modes (i.e., Cu cluster normal modes or phonons) as included in the EfHP approach, only results obtained with Bose–Einstein statistics are included in this work.

All quantum dynamical calculations, including the SCM and EfHP calculations, are performed using a (modified version) of the in-house TDWP code of the Leiden research group. The input parameters for these calculations can be found in the supplementary material. Surface configurations for the SCM are obtained using the in-house classical dynamics code,[24] while the surface configurations for the EfHP phonon calculations are obtained using atomic simulation environment (ASE).[61] The phonons and the corresponding thermal expansion are calculated within the quasi-harmonic approximation based on the finite displacement technique (using 0.01 Å displacements) as implemented in Phonopy version 2.18,[62,63]

in combination with LAMMPS of the March 28, 2023 version[64] or VASP 5.2.12[65–67] for the EAM and SRP48 results, respectively.

Due to the additional calculations required during propagation, as well as the larger grids needed, the EfHP calculation took about 20 days on a 32 core first generation EPYC CPU using OpenMP parallelization. In comparison, the BOSS and a single surface SCM calculation take about 1–2 days each on the same architecture. Note that the SCM results are an average of ∼100 runs on different distorted surface slabs. These runs are completely independent of each other and, thus, can be trivially parallelized with perfect scaling. This means that if enough computational resources are available, one would be able to get statistically converged SCM results within 2 days.

III. RESULTS AND DISCUSSION

A. Phonons and thermal expansion

One of the most important aspects of the surface potentials used is the thermal properties predicted for the Cu(111) surface, as outlined in Fig. 1(a). Here, we compare both the (a) linear thermal expansion coefficient α and the (b) lattice constant, as predicted by the EAM potential and the SRP48 functional, to the experimentally obtained values.[69] The theoretical values here are obtained by applying a quasi-harmonic approximation (QHA) to the calculated phonons, as outlined in Sec. II B. For the linear thermal expansion in Fig. 1(a), we see fairly good agreement between the experimental results and those obtained with the EAM potential. However, above ≈500 K, the EAM potential significantly deviates from the experiment. In contrast, the SRP48 obtained results do not agree that well with the experiment, overestimating the expansion across the entire temperature range. Nevertheless, SRP48 does better describe the curvature (but overestimates the actual value at all temperatures) of the experimental results even at higher temperatures, all the way up to the melting temperature of the Cu at around 1300 K.

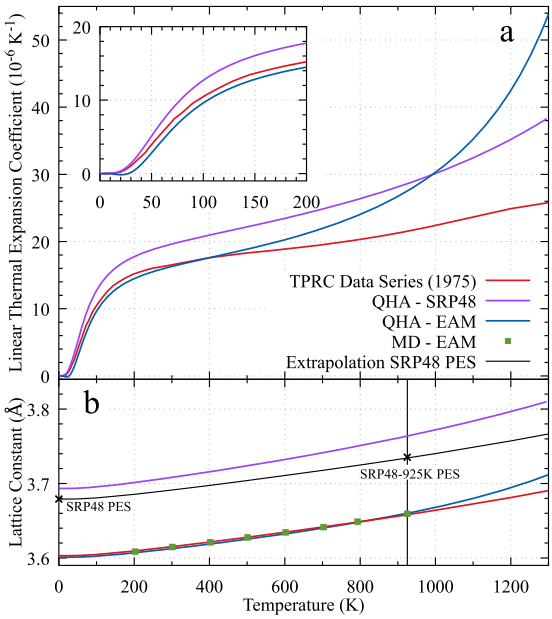

FIG. 1. Linear thermal expansion coefficient (a) and lattice constant (b) obtained using the quasi-harmonic approximation as implemented in phonopy for both the (purple) SRP48 functional with VASP and the (blue) Sheng *et al.*[68] EAM potential with LAMMPS. Results are compared to an aggregation of experimental results in red as published in Ref. 69. In (b), the lattice constants as used for construction of the SRP48 and SRP48-925K CRP PES are marked (black crosses), with a dashed curve guiding the eye for the applied extrapolation from 0 K using the experimental thermal expansion.[18] Also included in this sub-figure are lattice constants obtained with molecular dynamics, using the same EAM potential as was used for the QHA (green symbols).

These observations are also reflected in the predicted lattice constants, as shown in Fig. 1(b). Lattice constants obtained with the EAM potential agree well with those of the experiment, as one would expect as the potential was specifically fitted to reproduce these results.[68] This agreement also does not depend on whether a QHA or a molecular dynamics approach was used to obtain the reaction probabilities, which establishes the quality of the QHA approach for this system, at least up to 925 K. Again, SRP48 overestimates the lattice constant by a few percent across the entire temperature range, with a predicted 0 K lattice constant that is even higher than the experimentally obtained value at 1300 K. Furthermore, when constructing the CRP BOSS PES for the SRP48 functional, any zero-point energy (ZPE) effects were not taken into account while determining its lattice constant.[18] Consequently, when using the experimental thermal expansion curves to extrapolate to a 925 K lattice constant, as was done for the SRP48-925K CRP PES, these ZPE effects were not considered either.

In Table I, all lattice constants relevant to this study are shown. To match earlier works, phonon calculations for the SRP48 functional were performed using the CRP 925 K PES lattice constant, even though it does not match exactly our SRP48 QHA results. The deviation is small though, as shown in Fig. 1(b). Consequently, no additional rescaling is required for the H_2 c.m. coordinates to correct for the difference in lattice constant between the BOSS PES and the Cu surface phonon calculations performed for. This rescaling correction is done for the EAM phonon results and matches the approach used in the SCM.[21]

Having established the lattice constants that will be used for the different phonon calculations, we can now further investigate the effects the different surface potentials and lattice constants have on the surface phonons. In Fig. 2(a), we compare the frequency distributions of the surface normal modes of a Cu_{31} cluster, as used in previous studies,[27,30] to those obtained for a Cu(111) surface slab with the SRP48-925K CRP PES lattice constant, both calculated using the SRP48 DFT functional as the interatomic potential. We further compare the results for both the limited size

TABLE I. Overview of lattice constants of the different methods included in this work at a surface temperature of 925 K where appropriate.

Method	Lattice constant (Å)
SRP48 CRP[18]	3.6791
SRP48-925K CRP[18]	3.7352
QHA EAM[68]	3.6595
Cu_{31} cluster[27]	3.7100
Experiment[69]	3.6581

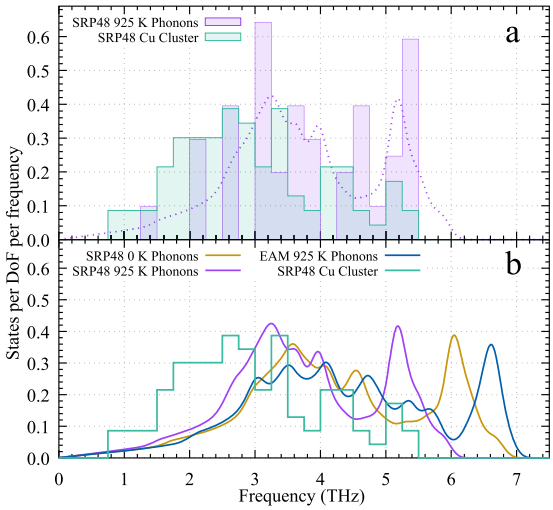

FIG. 2. Frequency distribution of the phonons calculated for the (purple) SRP48 925 K, (orange) SRP48 0 K, and (blue) EAM 925 K $3 \times 3 \times 1$ surface slab, as well as the (cyan) Cu_{31} cluster. In (a), the distribution for the finite size, as a histogram, is compared to the extrapolation to infinite size, represented by a dotted curve, for the phonon results. In (b), only the extrapolation to infinite size is shown for the phonon calculations, while the distribution for finite size is only shown for the cluster as a dotted histogram. The phonon and normal mode results for the SRP48 results were obtained using VASP, while the EAM results were obtained using LAMMPS. The Cu-cluster results were taken from Ref. 27 and calculated using the SRP48 functional in combination with VASP.

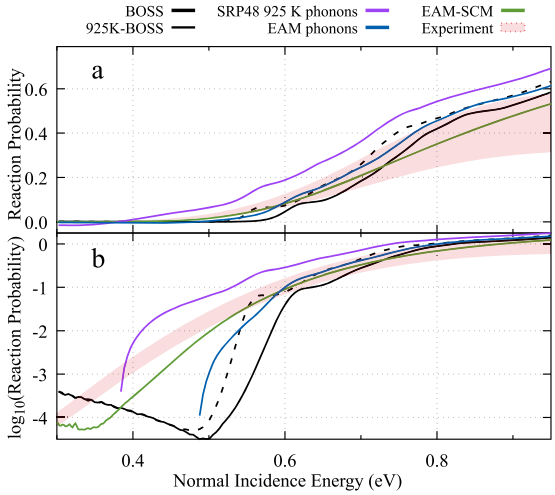

FIG. 3. Reaction probabilities for rovibrational ground state H_2 dissociating on a Cu(111) surface slab, obtained using a variety of methods on a linear (a) and a logarithmic (b) scale. Included are the ideal lattice BOSS and 925 K-BOSS results as a solid and dashed black curve, respectively. Effective Hartree potential results for the (purple) SRP48 925 K phonon and (blue) EAM phonon calculations. Results are also compared to EAM–SCM results from Ref. 29 and experimental results from Ref. 9. For the experimental results, a range of possible absolute saturation values is shown, as done in Ref. 29.

supercell used and those obtained when the frequencies are extrapolated to infinite size cells (in the case of the phonon calculations). The frequency distributions we find for the Cu cluster and the (infinite) phonon surface show some very clear differences. In particular, the phonon calculations predict a much larger fraction of relatively high frequency modes when compared to the cluster. The cluster then, instead, has many more modes at very low frequencies. These could have an effect on the dissociation, as these frequencies directly impact the importance of the effective Hartree potential on the H_2–Cu interaction. Furthermore, for both methods, we see good agreement between the extrapolated distributions and the finite-size histogram visualization.

Comparing the different phonon results, as outlined in Fig. 2(b), we note that increasing the lattice constant from 0 K to the 925 K SRP48 results decreases the highest frequencies present in the system. Interestingly, then, this does not seem to apply for the EAM calculated phonons, which were obtained for even larger lattice constants but with a different surface potential. Thus, it appears both the lattice constant and the surface potential play vital roles in these results. Nevertheless, all different phonon calculations show a similar distribution of frequencies, but with different maximum values, with very clear, broad peaks in the 3–4 THz range and a much sharper peak at the higher frequency between 5 and 7 THz, depending on the specific model.

B. Reactive scattering

How much these different frequency distributions affect the H_2/Cu(111) reaction has been investigated using several TDWP calculations. The most obvious choice then is, of course, the dissociation probability, as shown in Fig. 3. Here, we compare not only to the ideal, static surface BOSS model for both the 0 and 925 K SRP48 CRP PES but also to experimental results by Kaufmann *et al.*[9] and to QD results obtained using a sudden approximation implemented through the SCM as demonstrated by Somers and co-workers.[28,29,31] We furthermore also visualize the uncertainty in the experimental dissociation curves due to being unable to obtain absolute saturation values using the same method as described in Ref. 29. The slow increase in reactivity found for the BOSS results at low incidence energies is likely caused by errors within the split-operator method used, as investigated in more depth in Ref. 31.

In general, a clear increase in reaction curve broadness is found when applying the EfHP approach, with reactions starting at lower energies but then leveling off slower. This is especially obvious when results are plotted on a logarithmic scale in Fig. 3(b). Furthermore, the reaction appears to also start earlier regardless of the surface distortions added to the model, with the SRP48-925K curves showing the biggest shift toward lower energies. This shift in reaction onset can only be partially explained by the change in lattice constant of the BOSS PES, as can be seen by comparing the SRP48 BOSS and SRP48-925K BOSS results, in black and dashed black, respectively. Nevertheless, the broadening of the reaction curves by the EfHP method does not seem to quite match that of the experimental results, showing quite a rapid decay to no reaction at very low energy. This effect appears to be somewhat better described by the SCM, although the SCM (at a QD level) also slightly underestimates the curve onset of the experimental results.[29]

Comparing the reaction probabilities obtained for the 925 K SRP48 and EAM phonon EfHP results, there does not appear to be

a better approach. Results obtained for the 925 K SRP48-calculated phonons overestimate the experimental results across the entire energy range investigated, while those obtained using the EAM-calculated phonons underestimate the experiment at least for the lower energies. The SRP48 phonons results, however, do seem to match the curvature of the experiment slightly better. Furthermore, Sah *et al.*[32] show that using a Maxwell–Boltzmann distribution for the EfHP calculations instead of the Bose–Einstein distribution used in this work also has a significant effect on the trends found for the reaction probabilities, including the threshold for reactions moving to higher collision energies.

Another interesting aspect of the different methods we can look at is the state-to-state scattering of the H_2 molecule from the surface. In Fig. 4, we show the scattering to the rovibrational ground state $J = 0$, as well as the first available rotationally excited state $J = 2$. Overall, little difference is found between the different EfHP and BOSS PES results for both these scattering probabilities, with a smaller difference found for the rovibrationally elastic results. Each curve shows similar noise, likely partially due to imperfections of the PES, although at slightly different energies. In contrast, the SCM results do show a somewhat different curve. They also display less of the noise, which can be easily explained as the SCM curves are an average of several different distorted surfaces.[29]

C. Diffraction

Diffraction is a quantum mechanical phenomenon that has been observed in experiments with H_2 molecular beams scattering from Cu surfaces.[70,71] Unfortunately, to the best of our knowledge, there is no experimental data available specifically for Cu(111) at a 925 K surface temperature. Nevertheless, it is interesting to extract results for diffraction from our calculations done with the quantum dynamical methods used in this study: They all "naturally" include a proper description of diffraction, i.e., without introducing additional approximations as required with (quasi-)classical dynamics and implemented in the form of a particular binning scheme, but differ in the description of the increased surface corrugation at 925 K.[72,73]

Figure 5 compares results for the zeroth order specular diffraction peak [Fig. 5(a)] and the sum of the six first order peaks [Fig. 5(b)] as a function of normal incidence energy (and, thus, associated de Broglie wavelengths) of the incoming H_2 molecules. At a surface temperature of 0 K, both the EfHP and SCM methods reduce toward the BOSS case, i.e., the H_2 molecules scatter from surface atoms, which are all in their perfect lattice positions (black solid lines in Fig. 5). Slightly increasing the surface lattice constant to its value at 925 K without further perturbing the surface atom positions results in a small shift of the BOSS curves to lower energies corresponding to higher de Broglie wavelengths (black dashed lines in Fig. 5). This is as expected according to Bragg's law for monochromatic perfect sinusoidal waves, a superposition of which forms the wave packets describing the H_2 molecules in the quantum dynamical calculations.

Similar to the rovibrational scattering, we see little difference between the BOSS compared to both EfHP-based results at a phonon temperature of 925 K (black vs purple and blue solid lines in Fig. 5, respectively). It is interesting to note that peak positions and the general shape of the curves appear to be determined by V_0. For phonons calculated with the SRP48 functional and added to the SRP48 interaction potential obtained with the expanded lattice constant, the resulting curves closely follow the shape of the corresponding BOSS calculations (purple solid lines vs black dashed lines). The same

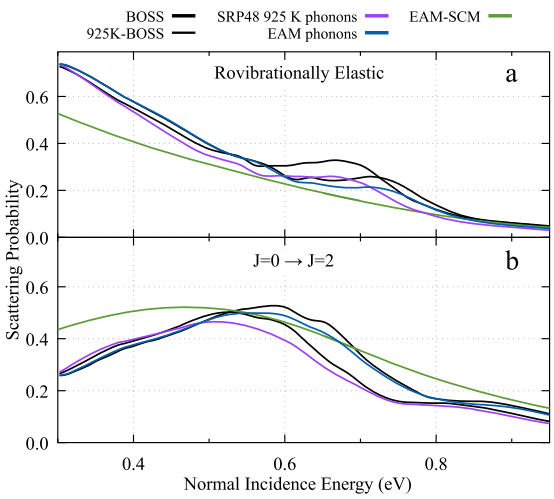

FIG. 4. Scattering probabilities for rovibrational ground state H_2 interacting with a Cu(111) surface slab, obtained using a variety of methods, for the (a) rovibrationally elastic and (b) J = 0 to J = 2 rotationally inelastic scattering. Included are the ideal lattice BOSS and 925 K-BOSS results as a solid and dashed black curve, respectively. Effective Hartree potential results for the (purple) SRP48 925 K phonons and (blue) EAM phonon calculations. Results are also compared to EAM–SCM results from Ref. 29.

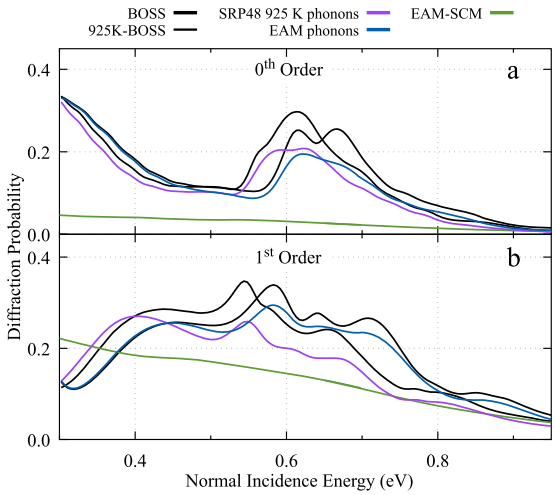

FIG. 5. Diffraction probabilities for rovibrational ground state H_2 interacting with a Cu(111) surface slab, obtained using a variety of methods, for the (a) specular and the (b) first order diffraction channel. Included are the ideal lattice BOSS and 925 K-BOSS results as a solid and dashed black curve, respectively. Effective Hartree potential results for the (purple) SRP 925 K phonon and (blue) EAM phonon calculations. Results are also compared to EAM–SCM results from Ref. 29. Implications for the surface temperature dependence of the attenuation of the diffraction probabilities are discussed in the text.

holds for adding the EAM phonons to the SRP48 interaction potential without accounting for lattice expansion (blue solid lines vs black solid lines). Both EfHP results show somewhat lower probabilities across all energies, but these can be easily explained by the higher reaction probabilities predicted (see Sec. III B). Irrespective of the metal–metal interaction potential determining the phonons, the extra surface corrugation introduced by going from 0 to 925 K phonon temperature is rather limited within the EfHP quantum dynamics. In stark contrast, the SCM quantum dynamics results obtained with the sudden approximation do show a very clear effect, particularly for the specular peak (green solid line vs black lines in Fig. 5). Second order diffraction results showed a similar behavior to the first order peaks for all methods we discuss. These results are included in the supplementary material, where we also plot the second and first order diffraction probabilities relative to the specular diffraction channel.

A rationalization for why the sudden approximation yields much more pronounced thermal effects for diffraction at these high temperatures is found in the way these methods describe the effects of surface temperature. As the EfHP averages over the relatively slow motion of the surface atoms relative to the H_2, the atoms are on average described around their ideal lattice positions and are, thus, mostly treated as such when looking at the H_2–Cu interaction. In contrast, the SCM averages over different displaced surfaces and the effect each of them has on the total result. Thus the H_2–Cu interactions are mostly considered when looking at surfaces heavily displaced by thermal effects, which will likely result in a strong decrease in the intensity of the specular diffraction peaks.

The massive decrease in the zeroth order diffraction probabilities agrees with an expected thermal attenuation effect, which has been observed in various molecular beam experiments.[70,71] In addition to a qualitative indication, it might be possible to make a quantitative comparison with experimental data in the future. In fact, Chadwick and Alexandrowicz[11] have measured off-normal diffraction of H_2 from Cu(111) for initially J = 1 and for surface temperatures between 150 and 500 K. On the other hand, our calculations for H_2 in its rovibrational ground state with a (modeled) surface temperature of 925 K were motivated by our (initial) interest in and experiments available for dissociation at this surface temperature. Furthermore, the experiments were performed for incidence energies well below our initial wave packet range. It is thus a significant computational endeavor to run EAM–SCM calculations for these low incidence energies. A time step smaller by a factor of ten would be required to rule out any numerical errors in computing these diffraction probabilities.[31] Similarly, additional calculations using the EAM–SCM within the sudden approximation would be required to investigate how these results change when the surface temperature is lowered below 925 K. Previous work by Smits and Somers[24] suggests that the approach used therein is unable to accurately reproduce the Cu surface below the copper Debye temperature of 300 K. In particular, the 925 K surface configurations have been constructed by molecular dynamics with the EAM potential using a thermostat that rescales velocities. This approach does not work well for low temperatures, as the thermostat artificially removes zero point energy from the solid. Therefore, a different approach to generating surface configurations is required for such low surface temperatures. In contrast, the EfHP approach might be more suited within this temperature range, as it does not use a thermostat that rescales velocities.

IV. CONCLUSION

In this work, we have presented a new look at the dissociation of H_2 from a thermally excited Cu(111) surface, using the effective Hartree potential (EfHP) approach with the SRP48 CRP PES. Previous iterations of the EfHP implementations have used the normal mode frequencies of a 31 atom copper cluster as a model to include the motion of the surface. Although a decent approximation, even previous studies already showed these clusters do not have the right distribution of frequencies one would expect for a surface. In this study, we, therefore, elect to use normal modes obtained from phonon calculations of a Cu(111) surface, calculated using the SRP48 DFT functional or an accurate EAM potential. The lattice constants used for these calculations are taken directly from those used to fit the potential energy surface (PES) for the SRP DFT results, to reduce the possibility of introducing errors. The phonon calculations using the EAM potential employ lattice constants obtained from this potential, with a correction added to the H_2 center of mass coordinates to account for this discrepancy between the PES and the surface potential. The frequencies obtained from these phonon calculations compared to those of the copper cluster showed a peak in the distribution at much higher frequency values, as was shown in a previous study. Furthermore, this frequency peak moved to lower frequencies as the lattice constant increased for the same potential. Nevertheless, the total effect depended much more on the potential used to calculate them, as the EAM results, with the lowest lattice constant, yielded a peak at the highest frequency.

Comparing the obtained dissociation probabilities, both for the ideal surface BOSS approach and the different EfHP results, we find a clear broadening of the reaction curve when the EfHP is included. This matches what one would expect from surface temperature, as some of the lowest reaction barriers are lowered while some of the highest reaction barriers are further increased. Interestingly, it appears the EfHP results are not significantly improved when the phonon frequencies are used over the cluster normal modes, with the used lattice constant being a much more deciding factor in agreement with experimental results. Nevertheless, the results obtained using the SRP DFT phonons at a lattice constant of 925 K do yield the broadest reaction curve.

The difference between the rovibrationally and vibrationally elastic scattering probabilities, obtained with and without the EfHP, is much less profound. The effects are overall very small, although the results that predict a higher reaction probability do also predict slightly lower scattering, as one should expect. The only clear outlier here are results obtained using a different method for including surface temperature, the static corrugation model (SCM), which predicts more energy exchange between the different degrees of freedom of the H_2 molecule, especially at lower incidence energies.

Looking at the 0th and first order diffraction probabilities, we first ascertain that increasing the lattice constant in the BOSS model shifts the diffraction peaks to lower incidence energies. Within the EfHP model, adding thermal disorder of the surface has a very small effect compared to the thermal lattice expansion, at best predicting slightly less diffraction as reaction probability increases. In contrast,

the SCM within the sudden approximation predicts very significant changes, with very strong attenuation effects greatly reducing diffraction of the 0th order and smaller effects at the 1st order. Although this is in qualitative agreement with trends observed in previous molecular beam experiments, a quantitative comparison with experimental data is currently not possible. The recent diffraction experiments for H_2 on Cu(111) by Chadwick and Alexandrowicz[11] have been carried out under significantly different conditions compared to the present calculations. Still, these experiments could pave the way toward an even better understanding of the approximations that are necessarily introduced when including surface motion into quantum-dynamical simulations of molecule–surface scattering.

Overall, we find that including the surface phonon frequencies in the EfHP approach over the normal modes of a Cu cluster does not significantly improve its results or its agreement with the experiment. Instead, it appears the H_2–Cu interaction potential and the lattice constant have a much larger impact on the results of the quantum dynamical calculations.

SUPPLEMENTARY MATERIAL

See the supplementary material for the computational details of the TDWP quantum dynamics simulations of H_2 dissociation on the Cu(111) surface.

ACKNOWLEDGMENTS

M.K.S. acknowledges the NBCFDC, Government of India, Ministry of Social Justice and Empowerment for the research fellowship. K.N. acknowledges IACS for the research fellowship. S.A. acknowledges DST-SERB, India, for research funding under Project No. CRG/2023/000611 and thanks IACS for access to the super-computing facility.

AUTHOR DECLARATIONS

Conflict of Interest

The authors have no conflicts to disclose.

Author Contributions

Bauke Smits: Conceptualization (equal); Data curation (equal); Formal analysis (equal); Investigation (lead); Methodology (equal); Software (supporting); Validation (lead); Visualization (lead); Writing – original draft (lead); Writing – review & editing (equal). **Mantu Kumar Sah**: Investigation (supporting); Software (supporting); Validation (supporting). **Koushik Naskar**: Investigation (supporting); Software (supporting); Validation (supporting). **Satrajit Adhikari**: Conceptualization (equal); Methodology (equal); Validation (supporting); Writing – original draft (supporting); Writing – review & editing (supporting). **Jörg Meyer**: Conceptualization (equal); Formal analysis (equal); Funding acquisition (lead); Methodology (equal); Project administration (equal); Resources (lead); Supervision (lead); Validation (equal); Writing – original draft (supporting); Writing – review & editing (supporting). **Mark F. Somers**: Conceptualization (equal); Data curation (equal); Methodology (equal); Project administration (equal); Software (equal); Supervision (equal); Validation (equal); Writing – original draft (supporting); Writing – review & editing (supporting).

DATA AVAILABILITY

The data that support the findings of this study are openly available in the research group's public repository at https://pubs.tc.lic.leidenuniv.nl/.

REFERENCES

[1] C. Smith, A. K. Hill, and L. Torrente-Murciano, "Current and future role of Haber–Bosch ammonia in a carbon-free energy landscape," Energy Environ. Sci. **13**, 331–344 (2020).
[2] I. Chorkendorff, *Concepts of Modern Catalysis and Kinetics* (Wiley VCH, Weinheim, 2003).
[3] H. F. Berger, M. Leisch, A. Winkler, and K. D. Rendulic, "A search for vibrational contributions to the activated adsorption of H_2 on copper," Chem. Phys. Lett. **175**, 425–428 (1990).
[4] H. A. Michelsen, C. T. Rettner, D. J. Auerbach, and R. N. Zare, "Effect of rotation on the translational and vibrational energy dependence of the dissociative adsorption of D_2 on Cu(111)," J. Chem. Phys. **98**, 8294–8307 (1993).
[5] C. T. Rettner, H. A. Michelsen, and D. J. Auerbach, "Quantum-state-specific dynamics of the dissociative adsorption and associative desorption of H_2 at a Cu(111) surface," J. Chem. Phys. **102**, 4625–4641 (1995).
[6] A. Hodgson, P. Samson, A. Wight, and C. Cottrell, "Rotational excitationand vibrational relaxation of H_2 scattered from Cu(111)," Phys. Rev. Lett. **78**, 963–966 (1997).
[7] H. Hou, S. J. Gulding, C. T. Rettner, A. M. Wodtke, and D. J. Auerbach, "The stereodynamics of a gas-surface reaction," Science **277**, 80–82 (1997).
[8] M. J. Murphy and A. Hodgson, "Adsorption and desorption dynamics of H_2 and D_2 on Cu(111): The role of surface temperature and evidence for corrugation of the dissociation barrier," J. Chem. Phys. **108**, 4199–4211 (1998).
[9] S. Kaufmann, Q. Shuai, D. J. Auerbach, D. Schwarzer, and A. M. Wodtke, "Associative desorption of hydrogen isotopologues from copper surfaces: Characterization of two reaction mechanisms," J. Chem. Phys. **148**, 194703 (2018).
[10] H. Chadwick, M. F. Somers, A. C. Stewart, Y. Alkoby, T. J. D. Carter, D. Butkovicova, and G. Alexandrowicz, "Stopping molecular rotation using coherent ultra-low-energy magnetic manipulations," Nat. Commun. **13**, 2287 (2022).
[11] H. Chadwick and G. Alexandrowicz,"Temperature dependent stereodynamics in surface scattering measured through subtle changes in the molecular wave function," Faraday Discuss. **251**, 76 (2024).
[12] C. Díaz, E. Pijper, R. A. Olsen, H. F. Busnengo, D. J. Auerbach, and G. J. Kroes, "Chemically accurate simulation of a prototypical surface reaction: H_2 dissociation on Cu(111)," Science **326**, 832–834 (2009).
[13] C. Díaz, R. A. Olsen, D. J. Auerbach, and G. J. Kroes, "Six-dimensional dynamics study of reactive and non reactive scattering of H_2 from Cu(111) using a chemically accurate potential energy surface," Phys. Chem. Chem. Phys. **12**, 6499–6519 (2010).
[14] M. Bonfanti, C. Díaz, M. F. Somers, and G.-J. Kroes, "Hydrogen dissociation on Cu(111): The influence of lattice motion. Part I," Phys. Chem. Chem. Phys. **13**, 4552 (2011).
[15] M. Wijzenbroek and M. F. Somers, "Static surface temperature effects on the dissociation of H_2 and D_2 on Cu(111)," J. Chem. Phys. **137**, 054703 (2012).
[16] F. Nattino, A. Genova, M. Guijt, A. S. Muzas, C. Díaz, D. J. Auerbach, and G.-J. Kroes, "Dissociation and recombination of D_2 on Cu(111): *Ab initio* molecular dynamics calculations and improved analysis of desorption experiments," J. Chem. Phys. **141**, 124705 (2014).

[17]M. Bonfanti, M. F. Somers, C. Díaz, H. F. Busnengo, and G.-J. Kroes, "7D quantum dynamics of H_2 scattering from Cu(111): The accuracy of the phonon sudden approximation," Z. Phys. Chem. **227**, 130617035227002 (2013).
[18]A. Mondal, M. Wijzenbroek, M. Bonfanti, C. Díaz, and G.-J. Kroes, "Thermal lattice expansion effect on reactive scattering of H_2 from Cu(111) at T_s = 925 K," J. Phys. Chem. A **117**, 8770–8781 (2013).
[19]G.-J. Kroes, J. I. Juaristi, and M. Alducin, "Vibrational excitation of H_2 scattering from Cu(111): Effects of surface temperature and of allowing energy exchange with the surface," J. Phys. Chem. C **121**, 13617–13633 (2017).
[20]P. Spiering and J. Meyer, "Testing electronic friction models: Vibrational de-excitation in scattering of H_2 and D_2 from cu(111)," J. Phys. Chem. Lett. **9**, 1803–1808 (2018).
[21]P. Spiering, M. Wijzenbroek, and M. F. Somers, "An improved static corrugation model," J. Chem. Phys. **149**, 234702 (2018).
[22]L. Zhu, Y. Zhang, L. Zhang, X. Zhou, and B. Jiang, "Unified and transferable description of dynamics of H_2 dissociative adsorption on multiple copper surfaces *via* machine learning," Phys. Chem. Chem. Phys. **22**, 13958–13964 (2020).
[23]O. Galparsoro, S. Kaufmann, D. J. Auerbach, A. Kandratsenka, and A. M. Wodtke, "First principles rates for surface chemistry employing exact transition state theory: Application to recombinative desorption of hydrogen from Cu(111)," Phys. Chem. Chem. Phys. **22**, 17532–17539 (2020).
[24]B. Smits and M. F. Somers, "Beyond the static corrugation model: Dynamic surfaces with the embedded atom method," J. Chem. Phys. **154**, 074710 (2021).
[25]E. W. F. Smeets and G.-J. Kroes, "Designing new SRP density functionals including non-local vdW-DF_2 correlation for H_2 + Cu(111) and their transferability to H_2 + Ag(111), Au(111) and Pt(111)," Phys. Chem. Chem. Phys. **23**, 7875–7901 (2021).
[26]E. W. F. Smeets and G.-J. Kroes, "Performance of made simple meta-GGA functionals with rVV10 nonlocal correlation for H_2 + Cu(111), D_2 + Ag(111), H_2 + Au(111), and D_2 + Pt(111)," J. Phys. Chem. C **125**, 8993–9010 (2021).
[27]J. Dutta, S. Mandal, S. Adhikari, P. Spiering, J. Meyer, and M. F. Somers, "Effect of surface temperature on quantum dynamics of H_2 on Cu(111) using a chemically accurate potential energy surface," J. Chem. Phys. **154**, 104103 (2021).
[28]B. Smits, L. G. B. Litjens, and M. F. Somers, "Accurate description of the quantum dynamical surface temperature effects on the dissociative chemisorption of H_2 from Cu(111)," J. Chem. Phys. **156**, 214706 (2022).
[29]B. Smits and M. F. Somers, "The quantum dynamics of H_2 on Cu(111) at a surface temperature of 925 K: Comparing state-of-the-art theory to state-of-the-art experiments," J. Chem. Phys. **157**, 134704 (2022).
[30]J. Dutta, K. Naskar, S. Adhikari, J. Meyer, and M. F. Somers, "Effect of surface temperature on quantum dynamics of D_2 on Cu(111) using a chemically accurate potential energy surface," J. Chem. Phys. **157**, 194112 (2022).
[31]B. Smits and M. F. Somers, "The quantum dynamics of H_2 on Cu(111) at a surface temperature of 925 K: Comparing state-of-the-art theory to state-of-the-art experiments 2," J. Chem. Phys. **158**, 014704 (2023).
[32]M. K. Sah, K. Naskar, S. Adhikari, B. Smits, J. Meyer, and M. F. Somers, "On the quantum dynamical treatment of surface vibrational modes for reactive scattering of H_2 from Cu(111) at 925 K," J. Chem. Phys. **161**, 014306 (2024).
[33]C. Carbogno, A. Groß, J. Meyer, and K. Reuter, "O_2 adsorption dynamics at metal surfaces: Non-adiabatic effects, dissociation and dissipation," in *Dynamics of Gas-Surface Interactions: Atomic-Level Understanding of Scattering Processes at Surfaces*, edited by R. Díez Muiño and H. F. Busnengo (Springer, 2013), pp. 389–419.
[34]G.-J. Kroes and C. Díaz, "Quantum and classical dynamics of reactive scattering of H_2 from metal surfaces," Chem. Soc. Rev. **45**, 3658–3700 (2016).
[35]G.-J. Kroes, "Computational approaches to dissociative chemisorption on metals: Towards chemical accuracy," Phys. Chem. Chem. Phys. **23**, 8962–9048 (2021).
[36]A. K. Tiwari, S. Nave, and B. Jackson, "The temperature dependence of methane dissociation on Ni(111) and Pt(111): Mixed quantum-classical studies of the lattice response," J. Chem. Phys. **132**, 134702 (2010).
[37]H. Guo, A. Farjamnia, and B. Jackson, "Effects of lattice motion on dissociative chemisorption: Toward a rigorous comparison of theory with molecular beam experiments," J. Phys. Chem. Lett. **7**, 4576–4584 (2016).
[38]B. Jackson, "Reduced density matrix description of gas–solid interactions: Scattering, trapping, and desorption," J. Chem. Phys. **108**, 1131–1139 (1998).
[39]B. Jackson, "The trapping of methane on Ir(111): A first-principles quantum study," J. Chem. Phys. **155**, 044705 (2021).
[40]B. Jackson, "Quantum studies of methane-metal inelastic diffraction and trapping: The variation with molecular orientation and phonon coupling," Chem. Phys. **559**, 111516 (2022).
[41]Y. Xiao, W. Dong, and H. F. Busnengo, "Reactive force fields for surface chemical reactions: A case study with hydrogen dissociation on Pd surfaces," J. Chem. Phys. **132**, 014704 (2010).
[42]A. Lozano, X. J. Shen, R. Moiraghi, W. Dong, and H. F. Busnengo, "Cutting a chemical bond with demon's scissors: Mode- and bond-selective reactivity of methane on metal surfaces," Surf. Sci. **640**, 25–35 (2015).
[43]G. N. Seminara, I. F. Peludhero, W. Dong, A. E. Martínez, and H. F. Busnengo, "Molecular dynamics study of molecular and dissociative adsorption using system-specific force fields based on ab initio calculations: CO/Cu(110) and CH_4/Pt(110)," Top. Catal. **62**, 1044–1052 (2019).
[44]G. J. Kroes, M. Wijzenbroek, and J. R. Manson, "Possible effect of static surface disorder on diffractive scattering of H_2 from Ru(0001): Comparison between theory and experiment," J. Chem. Phys. **147**, 244705 (2017).
[45]J. Meyer and K. Reuter, "Modeling heat dissipation at the nanoscale: An embedding approach for chemical reaction dynamics on metal surfaces," Angew. Chem., Int. Ed. **53**, 4721–4724 (2014).
[46]K. Shakouri, J. Behler, J. Meyer, and G.-J. Kroes, "Accurate neural network description of surface phonons in reactive gas–surface dynamics: N_2 + Ru(0001)," J. Phys. Chem. Lett. **8**, 2131–2136 (2017).
[47]K. Shakouri, J. Behler, J. Meyer, and G.-J. Kroes, "Analysis of energy dissipation channels in a benchmark system of activated dissociation: N_2 on Ru(0001)," J. Phys. Chem. C **122**, 23470–23480 (2018).
[48]J. Behler, "First principles neural network potentials for reactive simulations of large molecular and condensed systems," Angew. Chem., Int. Ed. **56**, 12828–12840 (2017).
[49]N. Artrith and J. Behler, "High-dimensional neural network potentials for metal surfaces: A prototype study for copper," Phys. Rev. B **85**, 045439 (2012).
[50]Q. Lin, L. Zhang, Y. Zhang, and B. Jiang, "Searching configurations in uncertainty space: Active learning of high-dimensional neural network reactive potentials," J. Chem. Theory Comput. **17**, 2691–2701 (2021).
[51]I. R. Craig and D. E. Manolopoulos, "Quantum statistics and classical mechanics: Real time correlation functions from ring polymer molecular dynamics," J. Chem. Phys. **121**, 3368–3373 (2004).
[52]Y. V. Suleimanov, F. J. Aoiz, and H. Guo, "Chemical reaction rate coefficients from ring polymer molecular dynamics: Theory and practical applications," J. Phys. Chem. A **120**, 8488–8502 (2016).
[53]R. A. Olsen, G. J. Kroes, O. M. Lo/vvik, and E. J. Baerends, "The influence of surface motion on the direct subsurface absorption of H_2 on Pd(111)," J. Chem. Phys. **107**, 10652–10661 (1997).
[54]M. D. Feit, J. A. Fleck, and A. Steiger, "Solution of the Schrödinger equation by a spectral method," J. Comput. Phys. **47**, 412–433 (1982).
[55]A. Vibok and G. G. Balint-Kurti, "Parametrization of complex absorbing potentials for time-dependent quantum dynamics," J. Phys. Chem. **96**, 8712–8719 (1992).
[56]G. G. Balint-Kurti, R. N. Dixon, and C. C. Marston, "Grid methods for solving the Schrödinger equation and time dependent quantum dynamics of molecular photofragmentation and reactive scattering processes," Int. Rev. Phys. Chem. **11**, 317–344 (1992).
[57]G.-J. Kroes and M. F. Somers, "Six-dimensional dynamics of dissociative chemisorption of H_2 on metal surfaces," J. Theor. Comput. Chem. **04**, 493–581 (2005).
[58]G.-J. Kroes, "Six-dimensional quantum dynamics of dissociative chemisorption of H_2 on metal surfaces," Prog. Surf. Sci. **60**, 1–85 (1999).
[59]H. F. Busnengo, A. Salin, and W. Dong, "Representation of the 6D potential energy surface for a diatomic molecule near a solid surface," J. Chem. Phys. **112**, 7641–7651 (2000).
[60]F. Nattino, C. Díaz, B. Jackson, and G.-J. Kroes, "Effect of surface motion on the rotational quadrupole alignment parameter of D_2 reacting on Cu(111)," Phys. Rev. Lett. **108**, 236104 (2012).

[61] A. Hjorth Larsen, J. Jørgen Mortensen, J. Blomqvist, I. E. Castelli, R. Christensen, M. Dułak, J. Friis, M. N. Groves, B. Hammer, C. Hargus, E. D. Hermes, P. C. Jennings, P. Bjerre Jensen, J. Kermode, J. R. Kitchin, E. Leonhard Kolsbjerg, J. Kubal, K. Kaasbjerg, S. Lysgaard, J. Bergmann Maronsson, T. Maxson, T. Olsen, L. Pastewka, A. Peterson, C. Rostgaard, J. Schiøtz, O. Schütt, M. Strange, K. S. Thygesen, T. Vegge, L. Vilhelmsen, M. Walter, Z. Zeng, and K. W. Jacobsen, "The atomic simulation environment – A python library for working with atoms," J. Phys.: Condens. Matter **29**, 273002 (2017).
[62] A. Togo, "First-principles phonon calculations with phonopy and Phono3py," J. Phys. Soc. Jpn. **92**, 012001 (2023).
[63] A. Togo, L. Chaput, T. Tadano, and I. Tanaka, "Implementation strategies in phonopy and phono3py," J. Phys.: Condens. Matter **35**, 353001 (2023).
[64] A. P. Thompson, H. M. Aktulga, R. Berger, D. S. Bolintineanu, W. M. Brown, P. S. Crozier, P. J. in 't Veld, A. Kohlmeyer, S. G. Moore, T. D. Nguyen, R. Shan, M. J. Stevens, J. Tranchida, C. Trott, and S. J. Plimpton, "LAMMPS - A flexible simulation tool for particle-based materials modeling at the atomic, meso, and continuum scales," Comput. Phys. Commun. **271**, 108171 (2022).
[65] G. Kresse and J. Hafner,"*Ab initio* molecular dynamics for liquid metals," Phys. Rev. B **47**, 558–561 (1993).
[66] G. Kresse and J. Furthmüller, "Efficient iterative schemes for *ab initio* total-energy calculations using a plane-wave basis set," Phys. Rev. B **54**, 11169–11186 (1996).
[67] G. Kresse and J. Furthmüller, "Efficiency of ab-initio total energy calculations for metals and semiconductors using a plane-wave basis set," Comput. Mater. Sci. **6**, 15–50 (1996).
[68] H. W. Sheng, M. J. Kramer, A. Cadien, T. Fujita, and M. W. Chen, "Highly optimized embedded-atom-method potentials for fourteen fcc metals," Phys. Rev. B **83**, 134118 (2011).
[69] Thermophysical Properties of Matter - The TPRC Data Series. Volume 12, Thermal Expansion Metallic Elements and Alloys, Technical Report, 1975.
[70] D. Farías and K.-H. Rieder, "Atomic beam diffraction from solid surfaces," Rep. Prog. Phys. **61**, 1575 (1998).
[71] M. F. Bertino and D. D. Farías, "Probing gas-surface potential energy surfaces with diffraction of hydrogen molecules," J. Phys.: Condens. Matter **14**, 6037 (2002).
[72] L. Bonnet, "Classical dynamics of chemical reactions in a quantum spirit," Int. Rev. Phys. Chem. **32**, 171–228 (2013).
[73] A. Rodríguez-Fernández, L. Bonnet, C. Crespos, P. Larrégaray, and R. Díez Muiño, "When classical trajectories get to quantum accuracy: The scattering of H_2 on Pd(111)," J. Phys. Chem. Lett. **10**, 7629–7635 (2019).